Magnetization transport across a ferromagnetic-paramagnetic interface

P. D. Sparks* and R. H. Silsbee

Laboratory of Atomic and Solid State Physics, Cornell University, Ithaca, New York 14853

(Received 10 February 1986; revised manuscript received 8 October 1986)

The transport of magnetization across a metallic ferromagnetic-paramagnetic bilayer is investigated using electron spin resonance. The ferromagnetic resonance and transmission electron spin resonance of films of palladium-iron alloys ($Pd_{100-x}Fe_x$, $0.5 \lesssim x \lesssim 4$) on copper foils are measured. The data are analyzed using a phenomenological model with two proposed mechanisms to couple the magnetizations in the film and the copper. One mechanism is the diffusion of electrons across the interface; the other is an exchange torque across the interface. The dominant coupling mechanism is found to be diffusion of electrons. The model, in addition, accounts well for the angular variation of the spin resonance signal at a fixed temperature. Finally it describes moderately well the variations with temperature of the spin resonance signal over the temperature range in which the magnetization and ferromagnetic resonance linewidth of the ferromagnetic film are varying dramatically.

I. INTRODUCTION

This paper describes an investigation of the transport of magnetization across a metallic ferromagnetic-paramagnetic interface. When there is good electronic contact between the metals, there is a coupling between the ferromagnetic resonance (FMR) and the conduction electron spin resonance of the paramagnet.[1,2] This coupling affects the magnitude, phase, and width of the transmission electron spin resonance (TESR) of a bilayer sample. The questions we address are the following: What is the microscopic origin of the coupling and how is it influenced by the bulk properties of the ferromagnet?

The initial results on conduction electron spin resonance (CESR) in a homogeneous metal[3] were explained by Dyson[4] in terms of the excitation in the skin depth of a spin eigenmode in the bulk of the paramagnetic metal. The same basic mechanism determines the transmitted signal through a plane slab of a pure metal.[5,6]

The CESR of coupled metallic systems has been studied using a variety of bilayer samples. The results for double layers of Al:Zn,[7] Cu:Li,[8-10] Mn:Li,[10] and Al:Na (Ref. 10) were interpreted in terms of surface relaxation at the interface[9,10] and by an appropriate averaging over the electronic properties of each layer.[8] To explain the TESR of Nb:Cu bilayers[11] required an analysis of the relaxation at the interface and of the relaxation via transmission of an electron into the niobium film and its subsequent relaxation. The latter process is affected by the properties of the niobium film.

By implanting ^{55}Mn ions in copper a different type of inhomogeneous material was made.[12] The analysis of the simple cases by Hurdequint[13] and Walker[14] showed two characteristics: the eigenmode for the CESR was determined by an averaging over the alloy properties and the magnitude of the response to the microwave excitation was determined by the susceptibility of the implanted layer.

The separation of the spin resonance response into the eigenmode and the characteristics of the excitation mech-

anism was exploited by Silsbee, Janossy, and Monod (SJM) (Ref. 2) in their study of ferromagnetic-paramagnetic bilayers. In SJM, the TESR of Permalloy, nickel, and iron films on copper was reported. They showed that the FMR determines the amplitude and phase of the enhancement of the TESR and developed a phenomenological theory to describe the bilayer. Their model for the coupling introduced a magnetization current due to the transmission of conduction electrons across the interface. The conduction electrons in the ferromagnet are polarized by the exchange field. The diffusion of those electrons into the copper provides a greater source of transverse magnetization than does the direct excitation by the microwave fields in the copper's skin depth.

In the experiments of SJM the ferromagnetic films were all materials with Curie temperatures well above room temperature, while the experiments were necessarily performed at 30 K or below in order to avoid excessive broadening of the TESR. This precluded the possibility of varying the important parameters of the ferromagnetic film, its magnetization $4\pi M$, and its ferromagnetic linewidth, in order to test the validity of the proposed model. Further, the strong FMR of the SJM samples detuned the microwave cavities so much that meaningful data could be obtained only with the FMR and TESR at very different fields. In the experiments described here, the Pd:Fe alloys have been specifically chosen to provide a Curie temperature near the experimentally available temperature range. In this way we have been able to follow the behavior of the coupled resonance over a wide range of the $4\pi M$ and FMR linewidth of the ferromagnetic films. An additional benefit was that the weak ferromagnetism allowed measuring the behavior of the coupled resonance for all achievable relative values of FMR and TESR resonant fields. These features of the current experiment have allowed a much more critical test of the phenomenological model of SJM.

The organization of this paper is as follows. Section II describes the phenomenological theory discussed by SJM

5198

and proposes an additional coupling mechanism via exchange torques across the interface. Section III contains the experimental details. In Sec. IV are the results for the FMR. The TESR results are in Sec. V. The conclusions are found in Sec. VI, which may be read first.

II. THEORETICAL MODEL

A phenomenological theory for a ferromagnetic-paramagnetic bilayer has been discussed by SJM. For the present work, we will briefly review that model focusing on the question of what information about the microscopic system is contained in the measured TESR. The coupling between the ferromagnet and the paramagnet is described by a boundary condition on the magnetization current at the interface between the metals and incorporates a phenomenological constant, Γ. The magnitude of Γ is a measure of the strength of the coupling. Whether it is real or imaginary is determined by the physical mechanism of the coupling.

A. TESR of the ferromagnetic-paramagnetic bilayer

The phenomenological theory of the response of a ferromagnetic film on a paramagnetic foil has been described by SJM. For the system under study here, with $4\pi M_0 \ll H_0$, the deviation of the direction of the magnetization in the ferromagnet from the direction of the applied field is small, a circumstance which allows substantial simplification of that analysis. The geometry is as shown in Fig. 1. A ferromagnetic film of thickness f is in contact with a paramagnetic foil of thickness p. The plane of the sample defines the x-y plane. The origin of the z axis is taken to be at the interface. We consider first the case of a static field of magnitude H_0 applied in the z direction. A circularly polarized microwave field of magnitude h is incident on the sample from the negative z direction.

The object of the calculation is to find the magnitude of
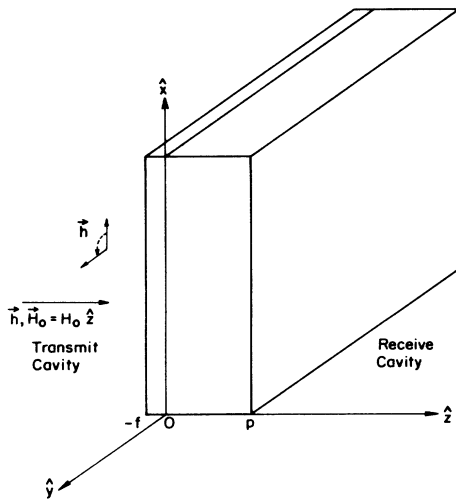
FIG. 1. Geometry for the bilayer calculation

the microwave field radiated from the vacuum surface of the paramagnet. However, from the solution for the TESR of a single foil,[11] it is known that the transmitted microwave field is proportional to the amplitude of the transverse magnetization at the back surface. Thus, for this calculation it suffices to find the amplitude of the transverse magnetization at $z = p$. The signal is then proportional to that amplitude. The constant can be calculated, but instead we will include it in the overall gain of the spectrometer when doing the data analysis.

The magnetization in the ferromagnetic film is modeled as arising from two sources: localized d-electron moments which comprise the ferromagnetic moment $\mathbf{M}$, and s-like conduction electrons. The uniform precession of the local moments is the ferromagnetic resonance. The conduction electrons are coupled by exchange to the localized moments. Since the magnetization of the conduction electrons is much less than the magnetization of the local moments, the effect of the s electrons on the d electrons is ignored. The s electrons in the ferromagnet are assumed to diffuse across the metallic interface into the paramagnet; diffusion from the paramagnet to the ferromagnet also occurs. This diffusion couples the magnetization in the two metals. The magnetizations may also be coupled by exchange, as will be explained below in the discussion of the boundary condition at the interface.

The motion of the conduction electrons in the ferromagnet and paramagnet are described by Bloch equations with diffusion, subject to the boundary conditions described below.

Specifically, the transverse magnetization is described by

$$\frac{dm_{x,y}}{dt} = \gamma(\mathbf{m} \times \mathbf{H})_{x,y} - \frac{(\mathbf{m} - \chi\mathbf{H})_{x,y}}{T_2} - (\nabla \cdot \mathbf{J}_m)_{x,y} , \quad (1)$$

where $\mathbf{H}$ is the applied field and $\mathbf{J}_m = -D\nabla(\mathbf{m} - \chi\mathbf{H})$ is the magnetization current. The other symbols have their usual meanings. It is the instantaneous nonequilibrium magnetization that enters the relaxation and diffusion terms.[15,16] The driving term for the conduction electrons in the ferromagnet is the rotating component of the exchange field, $\lambda\mathbf{M}$. That is, the conduction electrons are driven by the FMR. The resonant field for the s electrons in the ferromagnet is dominated by the static component of the exchange field, $\lambda\mathbf{M}_0$. The conduction electrons in the paramagnet are driven by the applied microwave field. The resonant field is set by the static applied field, H_0.

The Bloch equations for the rotating components of the conduction electrons's nonequilibrium magnetization become

$$[i(\gamma_f\lambda M_0 - \omega) + (1/T_f - D_f\nabla^2)]\delta m_f = i\omega\chi_f\lambda M^0 , \quad (2)$$

$$[i(\gamma_p H_0 - \omega) + (1/T_p - D_p\nabla^2)]\delta m_p = i\omega\chi_p h e^{-(1+i)z/\delta} , \quad (3)$$

where

$$\delta m_j \equiv \delta m_{jx} + i\delta m_{jy}; \quad j = p,f ,$$

$$\delta \mathbf{m}_j = \mathbf{m}_j - \chi_j\mathbf{H}_j ,$$

h is the amplitude of the applied microwave field, δ is the

skin depth in the paramagnet, and T_j, D_j, χ_j, γ_j are the T_2, diffusion constant, susceptibility, and gyromagnetic ratio for the conduction electrons in the ferromagnet and the paramagnet, and M^0 is the rotating component of the local moments's transverse magnetization (see Sec. II C). The assumption of the classical skin effect simplifies the calculation and only introduces a phase error of $\sim 15°$. The anomalous skin effect can be incorporated in an *ad hoc* manner at the end of the calculation.

At the metal-vacuum interfaces we assume there is no surface relaxation; $J_m = 0$ at $z = -f$ and p. We also assume that there is no surface relaxation at the metal-metal interface so $J_m \mid_{z=0^+} = J_m \mid_{z=0^-}$. The last boundary condition at the interface is that at $z = 0$,

$$J_m = \Gamma_0 \left[\frac{\delta m_f}{\chi_f} - \frac{\delta m_p}{\chi_p} \right] , \tag{4}$$

where δm_f (δm_p) and χ_f (χ_f) are the nonequilibrium magnetization and the susceptibility of the conduction electrons in the ferromagnet (paramagnet). The physical interpretation of Γ_0 will be discussed below. The argument for setting the magnetization current proportional to the difference in the scaled nonequilibrium magnetizations at the interface can be found in SJM.

B. Models for the mode coupling, Γ_0

We will present two models for the microscopic mechanism for the transfer of magnetization from the ferromagnet to the paramagnet. The first involves the diffusion of electrons across the interface for which Γ_0 is real. The second is based on an exchange interaction at the interface that produces a torque on the paramagnetic moments by the ferromagnet for which Γ_0 is imaginary.

For the mechanism of magnetization current via diffusion, Γ_0 can be estimated from a kinetic argument.[7,17] A rough estimate of Γ_0 gives

$$\Gamma_0 \propto \frac{\chi_f^0 v_{Ff} t_f}{4} = \frac{\chi_p v_{Fp} t_p}{4} , \tag{5}$$

where v_{Fi}, χ_i, and t_i are the Fermi velocity, susceptibility, and interfacial transmission coefficients for the conduction electrons in the ferromagnet (f) and paramagnet (p). The second equality is assured by detailed balance. The susceptibility enters through its proportionality to the density of states at the Fermi energy. In the paramagnet, it is the Pauli susceptibility; in the ferromagnet, it is the unenhanced Pauli susceptibility of the conduction electrons. The superscript on χ_f^0 is included to emphasize that this is not the total susceptibility of the conduction electrons.

The second model for the coupling is based on the effects of exchange between metals. Suppose the interface is considered to be a layer-one atomic cell thick in which the magnetization of one metal, **M**, and that in the other, **m**, can interact via exchange. Each magnetization will exert a torque on the other causing a transfer of angular momentum and hence magnetization across the interface. Initially, the two metals will be assumed to be both paramagnetic, then the extension to one being ferromag-

netic will be made.

The exchange torque per unit cell of the interface will be proportional to $J\mathbf{M} \times \mathbf{m} a^6/\beta^2$, where J is the exchange constant and a^3 is the cell volume. It will also be proportional to $J_m a^2$. Including the appropriate constants results[18] in an expression for Γ_0:

$$\Gamma_0 = i \frac{\gamma J a^4}{\beta^2} \chi_m M_0 , \tag{6}$$

where $\gamma = \beta/h$, β is the magnetic moment, and $M_0 = \chi_M H_0$ has been used for the ferromagnet.

The result of this heuristic argument is that if the magnetizations in the two metals are coupled via exchange, the phenomenological coupling constant will be imaginary rather than real as in the case of diffusive coupling.

To estimate the relative size of these two possible mechanisms, we use $M_0 \sim N\beta = \beta/a^3$, $\gamma = \beta/h$ and $a \propto 1/k_F$ to find

$$\frac{\Gamma_0''}{\Gamma_0'} \equiv \left| \frac{\Gamma_0(\text{torque})}{\Gamma_0(\text{diff})} \right| \propto \frac{J}{\varepsilon_F t} , \tag{7}$$

where ε_F is the Fermi energy. One might expect $0.01 \lesssim J/\varepsilon_F \lesssim 0.1$ so $\Gamma_0''/\Gamma_0' \lesssim 1$ as long as $t \gtrsim 0.1$. Thus, this theoretical model does not strongly determine the relative importance of the mechanisms.

C. Ferromagnetic resonance

For the purposes of this experiment, the ferromagnetic resonance (FMR) will be described by simple Bloch equations. With the assumptions that the film thickness is much less than the skin depth and that the internal magnetization is much less than the applied static field, both assumptions being applicable in this experiment, the rotating transverse component of the magnetization is given by

$$M^0 \equiv (M_x + iM_y)e^{-i\omega t}$$
$$= \frac{(iH_F + \Delta H_F)hM_0/H_F}{\Delta H_F + i(H_F - H)} , \tag{8}$$

where we have assumed a time dependence of $e^{+i\omega t}$ and h is the magnitude of the applied microwave field, M_0 is the internal magnetization, $\Delta H_F = 1/\gamma_F T_F$ is the half width at half maximum of the FMR line, and H_F is the resonant field. We note that H_F is the magnitude of the applied field at which resonance occurs. It is a function of the frequency of the microwave field, the internal magnetization and the demagnetizing factors.

For a plane slab, $H_F = H_\perp = \omega/\gamma_F + 4\pi M_0$ for $\mathbf{H}_0$ perpendicular to the slab, and

$$H_F = H_{||} = \{ -2\pi M_0 + [(2\pi M_0)^2 + \omega^2/\gamma_F^2]^{1/2} \}$$

when $\mathbf{H}_0$ is parallel to the slab. By measuring the FMR with the applied field perpendicular and parallel to the film, the internal magnetization and gyromagnetic ratio can be determined from

$$4\pi M_0 = \frac{1}{2} [2H_\perp + H_{||} - (5H_{||}^2 + 4H_{||}H_\perp)^{1/2}] ; \tag{9}$$

$$\gamma_F = \frac{\omega}{H_\perp - 4\pi M_0} .$$

In this experiment we will use the orientation dependence of the FMR in two ways. The first is to measure the magnetization and g value of the ferromagnetic film. The second is to exploit the fact that a particular value of H_F can be associated with many combinations of M_0 and field orientation. For example, a coincidence of the resonant fields for the FMR and the TESR can be obtained for a large M_0 with the field nearly parallel to the sample or a small M_0 with the field close to perpendicu-

lar. This will be used to distinguish the effects on the TESR of the magnitude of M_0 and the alignment of the TESR and FMR field.

D. Solution for TESR of bilayer

Combining the coupled Bloch equations with the boundary conditions gives the solution for the magnitude of the magnetization at $z = p$,

$$B_p = \frac{i\omega h \left[\dfrac{i\Gamma_0\Upsilon\delta^2}{D_p} + \dfrac{\chi_p\delta(1+i)}{2} + \dfrac{i\Gamma_0\Upsilon\lambda M_0}{\Omega_f} \dfrac{(i\gamma_F H_F + 1/T_F)}{\Omega_F H_F} \right]}{D_p k_p \sinh(k_p p) + \dfrac{\Gamma_0\Upsilon}{\chi_p}\cosh(k_p p)} , \tag{10}$$

with

$$\Upsilon = \frac{D_f k_f \sinh(k_f f)}{D_f k_f \sinh(k_f f) + (\Gamma_0/\chi_f)\cosh(k_f f)} ,$$

$$D_j k_j^2 = 1/T_j + i(\gamma_j H_{jz} - \omega) \equiv \Omega_j \text{ for } j = f, p ,$$

$$H_f = \lambda M_0 \text{ and } H_p = H_0 .$$

The first term in the numerator of Eq. (10) is smaller than the second unless the mean free path in the paramagnet is less than the skin depth. In this experiment, the conditions for the anomalous skin effect prevail, so the first term will be ignored.

The second term in the numerator of Eq. (10) is the amplitude of the magnetization driven directly by the applied microwave field. The third term is the amplitude driven

by the FMR. A comparison of the amplitude of the TESR with a ferromagnetic layer present to that without shows experimentally that the third term dominates. Therefore only the coupling to the FMR will be considered in the rest of this analysis.

The phenomenological constant Γ_0 always appears in this equation modified by Υ. We will define the effective coupling by $\Gamma \equiv \Gamma_0\Upsilon$. In most of the analysis, the factors Γ_0 and Υ cannot be disentangled.

The resulting expression for B_p has the form of a driving term determined by the FMR and a TESR denominator modified by a term proportional to the coupling Γ. To determine Γ involves fitting the data to the expression in Eq. (10). However, it is useful to examine the resonance denominator in the limit of $|k_p p| \ll 1$. Then

$$D_p k_p \sinh(k_p p) + \frac{\Gamma}{\chi_p}\cosh(k_p p) = p\left[1 + \frac{\Gamma p}{2\chi D}\right]\left[i(\omega - \gamma_p H_0) + \frac{1}{T_p} + \frac{\Gamma}{\chi_p}\left[1 + \frac{\Gamma p}{2\chi_p D_p}\right]^{-1}\right] . \tag{11}$$

The line shape would be Lorentzian, ignoring the possible field dependence in Γ.

There are two important limiting cases defined by the size of $\Gamma p/2\chi_p D_p$. In the weak-coupling limit, $|\Gamma p/2\chi_p D_p| \ll 1$, the effective relaxation rate is

$$\frac{1}{T_p'} = \frac{1}{T_p} + \frac{\Gamma'}{\chi_p p} , \tag{11}$$

where Γ' is the real part of Γ. The effective value of γ_p is

$$\gamma_p' = \gamma_p - \frac{\Gamma''}{\chi_p p H_0} , \tag{12}$$

where Γ'' is the imaginary part of Γ. That is, any coupling via diffusion will broaden the line and any coupling via exchange will shift the resonance. The magnitude of B_p will also be proportional to the magnitude of the coupling through the factor of Γ in the numerator.

These intuitive results do not hold in the strong-

coupling limit of $|\Gamma p/2\chi_p D_p| \gg 1$. In the strong-coupling limit, there is no shift in the resonance, and the effective relaxation rate is

$$\frac{1}{T_p'} = \frac{1}{T_p} + \frac{2D_p}{p^2} . \tag{13}$$

The line is broadened by the diffusion of electrons, excited in the skin depth, across the sample for Γ both real and imaginary. In addition, the magnitude of B_p is independent of Γ because the factors of Γ in the numerator and denominator cancel.

The implications of the weak and strong-coupling limits for the interpretation of TESR data is that measurements of the linewidth and gyromagnetic ratio do not automatically determine $\Gamma/1\chi_p$, even when T_p is known. One must first determine whether the weak or strong limit is applicable. In the weak limit, $\Gamma/1\chi_p$ can be determined. In the strong limit, only a lower bound on $|\Gamma/1\chi_p|$ is determined.

Similar weak- and strong-coupling limits can be defined in the thick limit where $|k_p p| \gg 1$. The line shape in these limits is also nearly independent of the magnitude of the coupling. Numerical calculations[18] of TESR line shapes over a wide range of values of $|k_p p|$ and $\Gamma p / 2 X_p D_p$ show that any given TESR line can be simulated quite well by a variety of sets of parameters: Γ / X_p, T_p, D_p, and amplitude. As a consequence the determination of a correct set of microscopic parameters from a single measured TESR line is typically not possible.

To complete the qualitative discussion of the expression for B_p we will examine Υ and provide some insight into the numerator. The quantity Υ is a measure of the effect on the conduction electrons in the ferromagnet of the interfacial coupling to the paramagnet. Strong- and weak-coupling limits for the conduction electrons in the ferromagnet can be defined as conditions on $\Gamma_0 k_f / X_f D_f$ or $\Gamma_0 / X_f D_f f$. In the limit of weak coupling, Υ becomes equal to 1, and the effective coupling Γ is independent of the ferromagnetic conduction electron dynamics. If Γ_0 is large, then $\Upsilon \sim 1 / \Gamma_0$, and Γ is independent of Γ_0. We will not discuss here the estimates of the form of Υ.[18] However, we note that if the coupling is not weak, then the temperature dependence of Υ can cause a temperature dependence in Γ which is not associated with any change of the of the characteristics of the interface.

For most ferromagnets $\Omega_f \sim \gamma_f \lambda M_0$, because the precession in the exchange field is more rapid than the relaxation rate. In that case, the FMR driving term is independent of M_0, and the amplitude and phase of B_p are determined by the FMR denominator, Ω_F. As the temperature approaches the Curie temperature of the ferromagnet, the linewidth of the FMR increases. Therefore, the magnitude of the driving term will decrease.

This expression for B_p has been derived by assuming the static field was perpendicular to the plane of the sample. To extend this result to arbitrary orientations of the applied field, as long as $4\pi M_0 \ll H_0$, it is only necessary to set H_F equal to the FMR field for the chosen orientation. Because H_F is a function of θ, the driving term will depend on θ. In particular, when the FMR driving term dominates the direct coupling to the microwaves, the amplitude and phase of the TESR will follow the amplitude and phase of the FMR at the TESR field as θ is varied. Because the angular variation of the H_F depends on the magnitude of M_0, this effect will be larger for large values of M_0. In analyzing the TESR data, we will look for an enhancement and apparent phase shift as θ is changed.

In our experiments at the lower temperatures, Ω_F may be varied in amplitude by a factor of up to 55% and in phase by up to 80° by changing the magnetic field orientation; the data are analyzed to confirm the predicted consequent variation in the TESR.

The analysis of the TESR data will first establish whether the paramagnet is in the weak- or strong-coupling limit. In the weak-coupling limit, a measurement of the ratio of the g shift to the line broadening is used to determine the ratio of Γ'' to Γ', and hence the relative importance of the two proposed coupling mecha-

nisms. Finally data at a number of temperatures will be analyzed in terms of the model to see whether a single set of parameters can successfully be used to describe the TESR through the temperature range in which the $4\pi M$ of the ferromagnet and the width of the FMR are changing dramatically.

III. EXPERIMENT

This experiment consisted of measurements of TESR and FMR on bilayers consisting of a ferromagnetic film on a paramagnetic foil. The paramagnet chosen was copper because it is easy to work with and is a simple metal whose TESR is well understood.[19] The ferromagnet was chosen from a series of alloys of palladium and iron (Pd:Fe). These alloys show a large variation of Curie temperature with iron concentration[20] which we have exploited to prepare alloys with T_C near the temperatures accessible for study by TESR. Because their g value is not too far from the value for copper, there is significant overlap of the FMR and the TESR even near T_C, and the analysis does not need to consider the complications involved in the coupling of resonances with different g values. The Pd:Fe alloys also have narrow FMR lines[21,22] and lower magnetic anisotropy than the alloys of Pd with the rest of the transition group. The problem with the Pd:Fe alloys is the poor reproducibility of the films, probably due to the difficulty of preparing homogeneous alloys.

The copper foils were cold rolled from 99.9999% pure electrodeposited slabs from Cominco American. Sequential rolling and vacuum annealing were required to obtain the final thickness of ~ 130 μm. The copper was not annealed after the final rolling. The defects introduced by the rolling increase the momentum scattering relative to the spin-flip scattering, and hence increase the TESR signal relative to the cyclotron background. The samples were given a light mechanical polish to remove some of the surface damage from the rollers.

The alloys were formed by arc melting in an argon atmosphere the correct mass ratios of Marz grade (99.99% pure) Pd and VP grade (99.95% pure) Fe obtained from the Materials Research Corporation. The alloy beads were cold rolled to ~ 120 μm thickness. Slivers of the alloy were cut to form the evaporation source.

The ferromagnetic films were deposited onto the copper foils using filament evaporation in a cryopumped vacuum system with a base pressure of 1×10^{-7} Torr. Immediately prior to the film deposition, the copper surface was ion milled in 3×10^{-5} Torr of high-purity argon to remove the top ~ 250 Å of the copper and, especially, the copper oxide. The 300-Å films were typically deposited in one minute. The peak pressure during the evaporation was 3×10^{-6} Torr. The samples were stored in liquid nitrogen, and warmed under a flow of dry nitrogen just before use. The sample was then mounted to form the common wall of two microwave cavities.

The measurements at 9.2 GHz were made on a superheterodyne spectrometer adapted to operate in reflection or transmission.[18] Two orthogonal phase components of the microwave signal were detected, digitized

TABLE I. FMR data summary

Sample No.	Composition and thickness	$4\pi M \mid_{4.2K}(G)$	$T_C(K)^a$	$\Delta H_{FMR} \mid_{4.2\,K}(G)^b$	g
1	$Pd_{96}Fe_4$ 450 Å	1050	110±5	225±25	2.13
2	$Pd_{99}Fe_1$ 700 Å	460 (5.7 K)	50±5	500±50 (5.7 K)	2.15
3	$Pd_{99}Fe_1$ 300 Å	130	13±3	600±60	
4	$Pd_{98}Fe_2$ 600 Å	475	65±5	330	2.18±0.01
5	0.99 at. % Fe 500 Å	310±20	55±5	260±25	2.18±0.02
6	0.99 at. % Fe 300 Å	375±25	60±10	280±25	2.19±0.01
7	0.44 at. % Fe 470 Å	185±15	25±1	250±25	2.21±0.02
8	0.70 at. % Fe 500 Å	200	15±3	240±25	2.19±0.02
9	0.95 at. % Fe 260 Å	515	>35	300±30	

[a]See text for determination of T_C.
[b]Averaged over field orientation.

by a Nicolet 1170 signal averager, and stored in a computer for later analysis. The data acquisition was triggered by a signal from an NMR field detector to provide a good field calibration.

IV. FERROMAGNETIC RESONANCE RESULTS

The FMR data were fit to a function of the form,

$$N = A \left[\frac{(H - H_F)\cos\phi + \Delta H \sin\phi}{(H - H_F)^2 + (\Delta H)^2} \right] + BH + C , \qquad (14)$$

where N is the number of counts in the digitized data,, A is the amplitude, ϕ is the microwave reference phase, ΔH is the half width at half maximum of the resonance, H_F is the resonant field, and B,C are constants included to accommodate a sloping baseline.

Of these fitting parameters only ΔH and H_F are of real interest. The fitting of the phase allowed taking data with arbitrary phase setting and avoided the need to symmetrize the FMR by adjusting the phase. In addition, the fitted phase was used as a consistency check on the fits: the fit was not accepted if the fitted phases of the orthogonal channels differed from 90° by more than 3°. The fits to the Lorentzian line shape were excellent for narrow lines, and less satisfactory as the linewidth approached 1000 G.

There was no angular variation of the linewidth to within the 10% experimental error. The temperature dependence of the linewidth is illustrated in Fig. 2. This result is in agreement with those of Bagguley and Robertson.[22] The linewidth is nearly constant until the temperature is near the Curie temperature, then it increases by approximately a factor of 3, until the resonance cannot be measured.

Calculating the $4\pi M$ through the angular variation of

the resonant field becomes less accurate with increasing temperature as the line broadens. A better relative measure of the magnetization at higher temperatures is obtained through its proportionality to the integrated intensity of the line. This, of course, is proportional to the product of the amplitude and the linewidth. In Fig. 3 are shown both the area and the $4\pi M$ computed from H_F at $\theta = 0°$ and 90°. The temperature at which the area goes to zero overestimates T_C because of the presence of the 3-kG applied field. The values of T_C in Table I are temperatures at which the resonance could not be measured. No attempt was made to fit these data to a theory.

The results for all the FMR measurements are summarized in Table I. The g values are in reasonable agreement
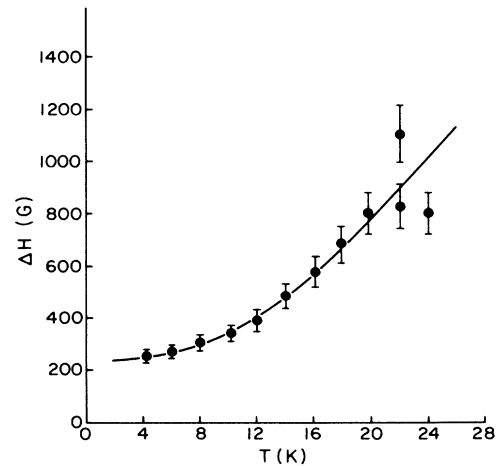
FIG. 2. Plot of FMR linewidth as a function of temperature for No. 7.
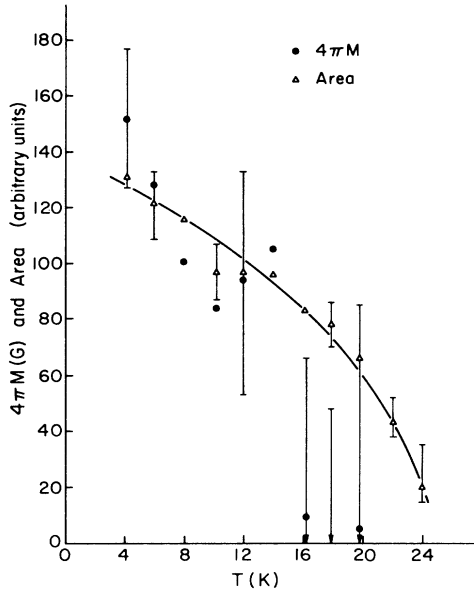
FIG. 3. Plot of the area under the FMR line and $4\pi M$ calculated from the orientation dependence of H_F as a function of temperature for No. 7. The area was scaled to a value of $4\pi M$ at approximately 7 K.

with reported values. The values of T_C as a function of iron concentration lie within the scatter of data from the literature,[20] i.e., the reproducibility of the alloy films was comparable with that of other investigators.

An unknown factor in this analysis is the homogeneity of the iron concentration in the ferromagnetic film. On one sample, No. 9, the FMR line became non-Lorentzian at higher temperatures. This may have been caused by a distribution of iron concentrations, hence a distribution of Curie temperatures and resonant fields, but this was not
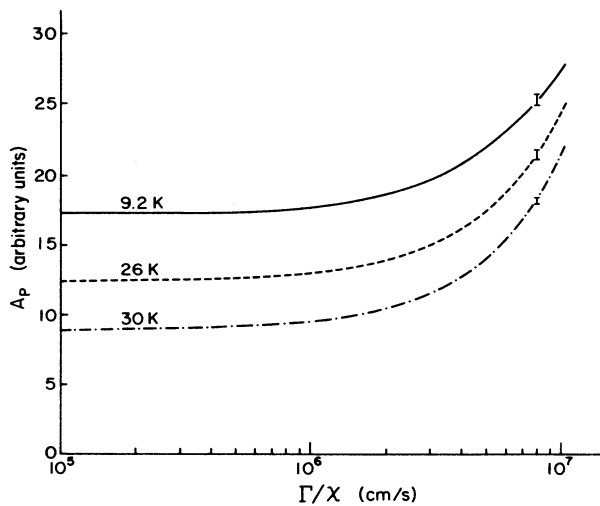
FIG. 4. A_p as a function of Γ/X for three temperatures for No. 6 for static field parallel to the plane of the sample.

confirmed by microscopic analysis. On the other samples there was no evidence in the FMR line shape to suggest the films were inhomogeneous.

V. TESR RESULTS

The data were initially analyzed by a computer fit to a function for the FMR coupled TESR with a linear background term:

$$N = \text{Re}(h_t)\cos\phi + \text{Im}(h_t)\sin\phi + a + bH ,$$

$$h_t = A_p \left[\frac{iH_F + \Delta H_F}{H_F[\Delta H_F + i(H - H_F)]} \right]$$

$$\times \left[\frac{1}{Dk \sinh(kp) + \Gamma/X\cosh(kp)} \right] , \qquad (15)$$

$$k = \left[\frac{1/T_2 + i(\omega - \gamma H)}{D} \right]^{1/2} ,$$

where we have dropped the subscript p from D, k, T_2, γ, and X. In this expression ω and p were input as fixed parameters appropriate to the sample and $H_F, \Delta H_F$ were determined by the FMR; however, this left eight unknowns: A_p, D, T_2, γ, Γ/X, ϕ, a, and b. It was not possible to fix D, T_2, and γ in the fitting routine because the fits were sensitive to variations in those parameters at levels below the certainty in their experimental determination. The quantity Γ was assumed to be real in the analysis of this experiment. The discussion in Sec. II D showed that an imaginary part of the coupling constant would appear as an effective shift in γ, if the paramagnet were in the weak coupling regime. Therefore, it is reasonable to assume that Γ in the fitting routine is real, and to look for any imaginary part in a g shift.

To understand the difficulties in fitting the data, recall that the line shape is relatively independent of the strength of the coupling. Many sets of the parameters $(A_p, D, T_2, \Gamma/X)$ can be used to fit the same line. Therefore a meaningful determination of those parameters requires some additional arguments. We will divide the analysis into the following sections: the angular dependence of the TESR at a fixed temperature, the determination of Γ/X, the ratio of Γ'' to Γ', and the temperature dependence of the TESR.

A. Angular dependence at fixed temperature

The TESR of copper is independent of the orientation of the magnetic field, ignoring the effects of the anisotropy of the diffusion constant. The TESR of the bilayer however shows large variations in amplitude, phase, and resonant field. To prove that our model of the coupling to the FMR adequately explains these effects, we fit the TESR data with and without including the FMR driving term.

The origins of the amplitude and phase dependence from our model were described in Sec. II D. To understand the variation in the resonant field note that for $1/\gamma T_2 \ll \Delta H_F$ and $|kp| \ll 1$, the measured TESR field becomes

$$H_0' = H_0 + (\gamma T_2 \Delta H_F)^{-1}(H_0 - H_F) \ .$$

That is, there is an apparent g shift with a sign determined by the relative positions of H_0 and H_F and a magnitude which may be as large as 20 G.

As expected, the fits to the data without the FMR term, the first set of parentheses of Eq. (15), show a strong dependence of γ and ϕ upon field orientation as described above. The quantitative analysis of the amplitude is hampered by the ambiguity in the set of parameters A_p, D, T_2, and Γ/χ, but if D, T_2, and Γ/χ are held fixed, then A_p also appropriately follows the magnitude of the FMR at the TESR field. However, when the measured FMR parameters are included in the analysis, γ, ϕ, and A_p become independent of θ. We conclude, therefore, that the coupling of the TESR is via the FMR, and that Eq. (15) adequately describes the coupling's dependence on the relative positions of the FMR and TESR fields.

Furthermore, the measured γ differs from γ_{Cu} by an amount corresponding to a field shift of less than 1 G. This may convey some information about the nature of the coupling, but only if the samples were weakly coupled, as discussed later.

B. Analysis for Γ/χ

As noted earlier, any given experimental line could be satisfactorily fit with a number of distinct sets of the parameters $(A_p, D, T_2, \Gamma/\chi)$. Some independent knowledge of T_2 was required in order to remove the ambiguity and to obtain information about Γ/χ. The procedure for the analysis for each TESR line was as follows. A number of distinct but physically reasonable values of Γ/χ were chosen and for each value the experimental line shapes were fit to the function in Eq. (15). To emphasize that the values for D, T_2, and A_p returned by the fitting routine are implicitly functions of the assumed Γ/χ, we will denote them by D^*, T_2^*, and A_p^*. The range of Γ/χ was limited by an upper bound of $\sim 4 \times 10^7$ cm/s, corresponding to an interfacial transmission probability equal to one,
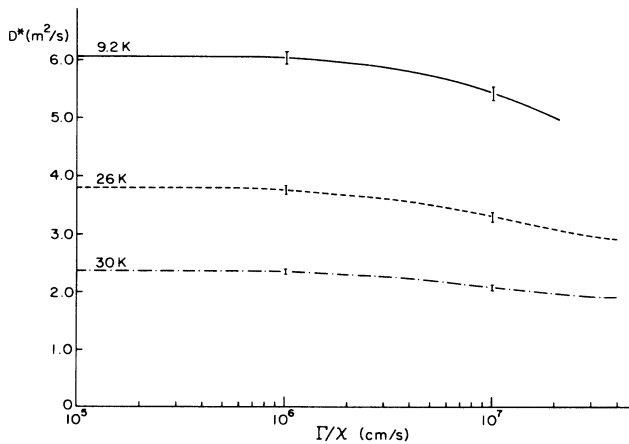
and was terminated at the lower end when the results became independent of the choice of Γ/χ.

In Figs. 4, 5, and 6 (for No. 6) are examples of plots of A_p, T_2^*, and D^* as a function of Γ/χ. Each line on the graphs represents values of the fitting variables for one TESR line. We notice that there are substantial ranges where the results are insensitive to the choice of Γ/χ. In particular, the values of D^* did not have a strong enough dependence on Γ/χ to determine Γ/χ.

The most important feature of the plot of T_2^* as a function of Γ/χ in Fig. 6 is the qualitatively different behavior at high and low temperatures. This is indicative of the differences between the weak and strong coupling at low and high temperatures, respectively, and shows that the shape of the plot of T_2^* versus Γ/χ can be used to estimate the strength of the coupling.

To justify this conclusion consider the thin limit, $p < (2DT_2)^{1/2}$, with a real Γ. Then the effective relaxation rate, $1/T_2'$ is given from Eqs. (11) and (13) by

$$1/T_2' = 1/T_2 + \Gamma/(\chi p) \quad \text{(weak limit)} \ ,$$

$$1/T_2' = 1/T_2 + 2D/p^2 \quad \text{(strong limit)} \ .$$

First suppose that the sample is in the strong-coupling limit. Then if one forces a fit with $\Gamma/\chi = 0$, one will find $T_2^* = T_2' < T_2$. As the parameter Γ/χ is increased, T_2^* will also increase. When Γ/χ is allowed to be large enough that the correct strong limit expression for T_2' is suitable, then the fit will give the correct value $T_2^* = T_2$ independent of Γ/χ. This describes the qualitative behavior of the 30 K data for T_2^* in Fig. 6.

Next suppose that the sample is weakly coupled. Then for Γ/χ less than the true value, the fit will yield $T_2^* < T_2$. At the true value of Γ/χ, the value of T_2^* will equal T_2. As the parameter Γ/χ is increased, the value of T_2^* will increase. However, when the input value of Γ/χ is sufficiently large that the strong limit expression for T_2' is applicable, and if $2D/p^2$ is greater than $1/T_2'$, then there is no value for T_2^* which can fit the line. This describes the behavior shown for the 9.2 K data in Fig. 6.

The real part of Γ/χ (or its lower bound) is determined

FIG. 5. D^* as a function of Γ/χ for three temperatures for No. 6 for static field parallel to the plane of the sample.
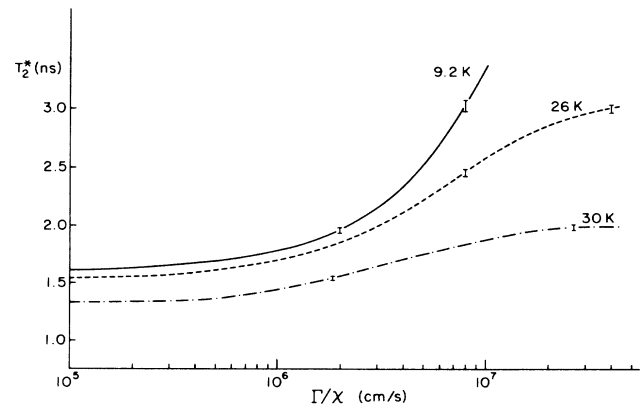
FIG. 6. T_2^* as a function of Γ/χ for three temperatures for No. 6 for static field parallel to the plane of the sample.

TABLE II. Low-temperature values of $\Gamma'/\mathcal{X}$ for weakly-coupled samples and $|\Gamma/\mathcal{X}|$ for strongly-coupled samples

Sample No.	Coupling	$\Gamma'/\mathcal{X}$ or $|\Gamma/\mathcal{X}|$ (10^6 cm/s)	t^a (%)
5	weak	6.2 ± 0.7	16 ± 2
6	weak	4.3 ± 0.7	11 ± 2
7	strong	$>2.7\pm0.3$	
8	almost strong	$>2.5\pm0.3$	
9	strong	$>3.0\pm0.3$	

[a]Computed using $v_F = 1.6\times10^8$ cm/s and Eq. (10).

from the plots of T_2^* as a function of $\Gamma/\mathcal{X}$ by the point at which $T_2^* = T_2$. For copper from the same batch as No. 5 and No. 6, the measured low-temperature value of T_2 was (2.5 ± 0.2) ns. This determines $\Gamma'/\mathcal{X}$ to be $(6.2\pm0.6)\times10^6$ cm/s for No. 5 and $(4.3\pm0.7)\times10^6$ cm/s for No. 6. The T_2 was not measured in the copper used for No. 7, No. 8, and No. 9. All these samples showed quite strong coupling so a lower bound on $|\Gamma/\mathcal{X}|$ was set using the condition that $|\Gamma p/2\mathcal{X}D| \approx 1$. Having determined $\Gamma/\mathcal{X}$, D and A_p are satisfactorily determined by the fits, and are, in fact, relatively insensitive to the choice of $\Gamma/\mathcal{X}$. The results for $\Gamma'/\mathcal{X}$ or $|\Gamma/\mathcal{X}|$ are summarized in Table II.

To demonstrate the consistency of using the shape of the plots of T_2^* as a function of $\Gamma/\mathcal{X}$ to determine the coupling, we note that for the lines shown in Fig. 6, the computed values of $\Gamma p/2\mathcal{X}D$ are 0.5, 0.9, and 1.5 for 9.2, 26, and 30 K, respectively. This shows good agreement between the qualitative features of the plots and the theoretical criterion of comparing $\Gamma p/2\mathcal{X}D$ with 1. The change in the shape of the curve occurs for intermediate coupling, as it should.

The analysis showed a considerable variation in coupling among various samples (see Table II), which is easily understood. The criterion for strong or weak coupling is a condition on the ratio $\Gamma p/2\mathcal{X}D$. For a fixed $\Gamma/\mathcal{X}$, a sample with a smaller diffusion constant will be more strongly coupled. This is consistent with the observation that the three samples with high resistivity were strongly coupled, while the low-resistivity samples were not. Also, as the temperature increases, the value of D decreases, and as shown in Fig. 6 the sample becomes more strongly coupled.

From $\Gamma'/\mathcal{X}$, the interfacial transmission probability can be computed using Eq. (5). The values of t are 10–15 % in reasonable agreement with those values determined in some other experiments,[2,8,11] but higher than in others.[10,23,24]

C. The ratio of Γ'' to Γ'

By finding $\Gamma'/\mathcal{X}$ for the weakly coupled samples we have determined that at least part of the coupling arises from the diffusion of electrons across the interface. To see whether there is also some coupling via torques, we note that the measured g value for No. 6 was 2.033 ± 0.0006. To convert this into a measure of Γ'' we use Eq. (12) and $g_{Cu}=2.033$. For No. 6, $f=9.2034$ GHz

and $p = 155$ μm so we compute $\Gamma''/\mathcal{X}\lesssim2.6\times10^5$ cm/s. The main caveat on this conclusion is that Eq. (6) is only valid for $p \ll (2DT_2)^{1/2}$ whereas this sample had $p \sim (2DT_2)^{1/2}$. Nevertheless, this provides a bound on the relative importance of the coupling via diffusion to the coupling via torques of $\Gamma''/\Gamma' <4\%$. We note that this is consistent with the theoretical estimate in Eq. (7).

The importance of the distinction between the strong- and weak-coupling limits was not recognized in SJM. Estimates of the relevant parameters indicate that in fact the thinner samples with Permalloy films were roughly at the crossover between the weak and the strong limits, and the thick sample was in the strong limit. As a consequence the quantitative conclusions for the coupling strength $\Gamma/\mathcal{X}$ for the thin samples are at best good to within only a factor of 2 and for the thick sample the quoted value is only a lower bound. Conclusions concerning the ratio Γ'/Γ'' must be correspondingly weakened. The remarks concerning the invariance of the peak signal amplitude with variable coupling strength require only the thin limit assumption and remain valid.

D. Temperature dependence

An examination of the temperature dependence of A_p^*, T_2^*, and D^* can help to distinguish further among values of $\Gamma/\mathcal{X}$ if $\Gamma/\mathcal{X}$ can be assumed to be temperature independent, or provide insight into the breakdown of the simple model if $\Gamma/\mathcal{X}$ is dependent on temperature.

There are two sources of temperature dependence of D^*, T_2^*, and A_p^* in our model. The first is the temperature dependence of D and T_2 in the paramagnet. By comparing the temperature dependence of D^* and T_2^* with the known behavior of D and T_2 we may obtain some information about $\Gamma/\mathcal{X}$. In the present experiment, the decrease in D^* with increasing temperature is consistent with the decrease of D as phonon scattering becomes important. However, the values of D^* are relatively insensitive to $\Gamma/\mathcal{X}$, so no information about $\Gamma/\mathcal{X}$ is obtained.

Similarly, the values of $1/T_2^*$ show the correct features for all $\Gamma/\mathcal{X}$ (see Fig. 7). They are independent of tem-
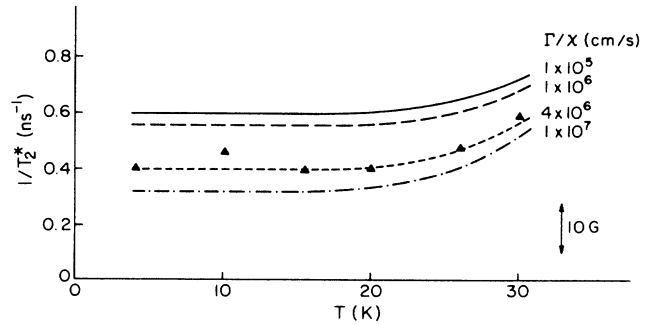
FIG. 7. $1/T_2^*$ as a function of temperature for four values of $\Gamma/\mathcal{X}$ for No. 6. The line labeled "10 G" shows the size of $1/T_2$ which corresponds to a half width at half maximum of 10 G ($\Delta H = 1/\gamma T_2 = 10$ G) for $g=2.033$. The data points are shown for only one value of $\Gamma/\mathcal{X}$.
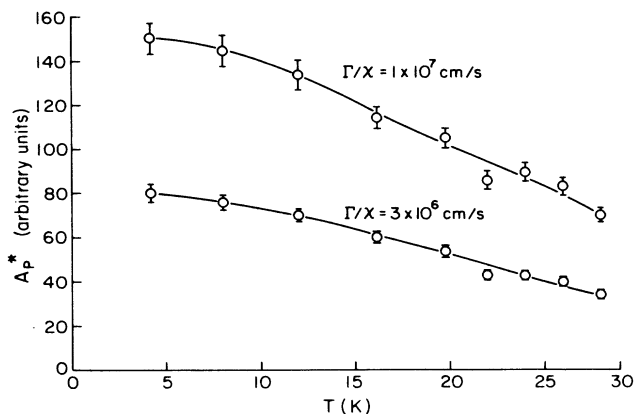
FIG. 8. A_p^* as a function of temperature for two values of Γ/χ for No. 7.

perature until about 20 K, and then show an additional relaxation due to phonons increasing the width by ~ 10 G at 30 K in agreement with the reported temperature dependence of T_2 in copper.[19]

In the simplest picture A_p is independent of temperature. This assumes that the bottleneck in the ferromagnet is not broken down ($\Omega_f \to \gamma_f \lambda M_0$) and that the ferromagnet is weakly coupled to the paramagnet ($\Upsilon = 1$). Then

$$A_p = \frac{\Gamma_0 \Upsilon \lambda M_0 A \gamma_f}{\Omega_f} \to \Gamma_0 A \ ,$$

where A is the effective spectrometer gain. In this case A_p is independent of M_0 and the dynamics of the conduction electrons in the ferromagnet. If either assumption breaks down, A_p can become dependent on temperature.

An example of the data for A_p^* as a function of temperature is shown in Fig. 8. For all the samples, the value of A_p^* at a fixed Γ/χ decreased with increasing temperature. We notice that despite a factor of 25 variation in $4\pi M$, a factor of 4 variation in ΔH_F, and a factor of 100 variation in the apparent strength of the TESR, the deduced A_p^* only varies by a factor of 2.

To see whether the residual temperature dependence of A_p is naturally explicable within our model we first looked at the breakdown of the bottleneck in the fer-

romagnet. Assuming the conduction electron dynamics in the ferromagnet are dominated by relaxation ($\Omega_f \to 1/T_f$) does not produce the observed results. Either a partial breakdown, or the presence of a significant magnetization directly driven by the microwave field can produce these effects. There would be phase shifts associated with either mechanism, and they should be investigated for data with good absolute phase information.

There are too many unknown parameters to examine a switch from weak to strong coupling of the ferromagnet to the paramagnet. Making a simplifying assumption of a single spin species in the ferromagnet[18] helps reduce the number of unknowns, but does not lead to the required temperature dependence in Υ.

VI. CONCLUSIONS

In summary, the TESR of a ferromagnetic-paramagnetic bilayer has been described as proposed by SJM in terms of a coupling constant, Γ, coupling the FMR in the film to the TESR in the paramagnet. Despite the apparent sensitivity of the line shape to Γ, the experiment is only sensitive to Γ when the sample is in a weak-coupling limit. For weakly coupled samples, the value of Γ was determined to yield the probability that an electron from the copper will enter the Pd:Fe film of $(13\pm2)\%$. An upper limit on the relative importance of coupling via exchange torques to coupling via electron diffusion is 4%. The phenomenological theory provides a good description for the TESR at a fixed temperature and describes, as well, the major portion of the temperature dependence. However, there is a residual temperature dependence of the amplitude of the TESR which is not completely explicable within the framework of the theory for temperatures at which the internal properties of the ferromagnet are changing. '

*Present address: Department of Physics, University at California-Irvine, Irvine, CA 92717.

[1]A. Janossy and P. Monod, Solid State Commun. 18, 203 (1976).

[2]R. H. Silsbee, A. Janossy, and P. Monod, Phys. Rev. B 19, 4382 (1979).

[3]G. Feher and A. F. Kip, Phys. Rev. 98, 337 (1955).

[4]F. J. Dyson, Phys. Rev. 98, 349 (1955).

[5]R. B. Lewis and T. R. Carver, Phys. Rev. Lett. 12, 693 (1964); Phys. Rev. 155, 309 (1967).

[6]N. S. Van der Ven and R. J. Schumacher, Phys. Rev. Lett. 12, 695 (1964).

[7]A. Janossy and P. Monod, J. Phys. F 3, 1752 (1973).

[8]L. D. Flesner, D. R. Fredkin, and S. Schultz, Solid State Commun. 18, 207 (1976).

[9]A. Janossy and K. Csermak, Hungarian Academy of Science, Budapest, Report No. KFKI-74-17 1974 (unpublished).

[10]Richard Magno and Joe H. Pifer, Phys. Rev. B 10, 3727 (1974).

[11]George W. Graham and Robert H. Silsbee, Phys. Rev. B 9, 4184 (1980).

[12]P. Monod, H. Hurdequint, A. Janossy, J. Obert, and J. Charmont, Phys. Rev. Lett. 29, 1327 (1972).

[13]H. Hurdequint, Thése de troiséme cycle, University of Paris, Orsay, 1973 (unpublished).

[14]M. B. Walker, Can. J. Phys. 52, 2065 (1974).

[15]H. C. Torrey, Phys. Rev. 104, 563 (1956).

[16]M. B. Walker, Phys. Rev. B 3, 30 (1971).

[17]M. R. Menard and M. B. Walker, Can. J. Phys. 52, 61 (1974).

[18]P. D. Sparks, Ph.D. thesis, Cornell University, 1983 (unpublished).

[19]S. Schultz and C. Latham, Phys. Rev. Lett. 15, 148 (1965).

[20]G. J. Nieuwenhuys, Adv. Phys. 24, 515 (1975).

[21]D. M. S. Bagguley and J. A. Robertson, Phys. Lett. 27A, 516 (1968).

[22]D. M. S. Bagguley and J. A. Robertson, J. Phys. F 4, 2282 (1974).

[23]B. Vigouroux and J. C. Gourdon, J. Phys. F 11, 1505 (1981).

[24]L. Allam and B. Vigouroux, Solid State Commun. 40, 955 (1981).